

Fluid - solid transition in simple systems using density functional theory

Atul S. Bharadwaj and Yashwant Singh

Department of Physics, Banaras Hindu University, Varanasi-221 005, India.

(Dated: October 17, 2018)

Abstract

A free energy functional for a crystal proposed by Singh and Singh (Europhysics Letters **88**, 16005 (2009)) which contains both the symmetry-conserved and symmetry-broken parts of the direct pair correlation function has been used to investigate the fluid-solid transition in systems interacting via purely repulsive WCA Lennard - Jones (RLJ) potential and the full Lennard - Jones (LJ) potential. The results found for freezing parameters for the fluid - face centred cubic (fcc) crystal transition are in very good agreement with simulation results. It is shown that although the contribution made by the symmetry broken part to the grand thermodynamic potential at the freezing point is small compared to that of the symmetry conserving part, its role is crucial in stabilizing the crystalline structure and on values of freezing parameters. The effect of attractive part of the LJ potential on the freezing parameters is found to be small, confirming the view that the fluid - solid transition is primarily determined by the repulsive part of the potential.

PACS numbers: 64.70.D-, 05.70.Fh, 63.20.dk

I. INTRODUCTION

The fluid-solid transition in three dimensions is a first order phase transition in which continuous symmetry of the fluid is broken into one of the Bravais lattices. The density functional theory (DFT) of freezing, first proposed in 1979 by Ramakrishnan and Youssuf (RY) [1] has extensively been used to study this transition. The central quantity in this theory is the reduced Helmholtz free energy of both the crystal, $A[\rho]$, and the fluid, $A(\rho_l)$ [2]. For a crystal, $A[\rho]$ is a unique functional of single particle density distribution $\rho(\vec{r})$ whereas for the fluid $A(\rho_l)$ is simply a function of fluid density $\rho_l (= N/V, N$ being the number of particles in volume V). The density functional formalism is used to find expression for $A[\rho]$ (or for grand thermodynamic potential) in terms of $\rho(\vec{r})$ and the direct pair correlation function (DPCF). Minimisation of this expression with respect to $\rho(\vec{r})$ leads to an expression that relates $\rho(\vec{r})$ to the DPCF [3]. The DPCF that appears in these expressions corresponds to crystal and is functional of $\rho(\vec{r})$. When this functional dependence is ignored by replacing the DPCF by that of the coexisting uniform fluid [1] or by that of an "effective uniform fluid" [4, 5], the free energy functional becomes approximate and fails to provide an accurate description of freezing transition for a large class of intermolecular potentials [6, 7].

A free energy functional in which the functional dependence of DPCF on $\rho(\vec{r})$ has been taken into account has recently been proposed [8, 9] and applied to steady freezing of fluids in two- and three-dimensions. The results found for the isotropic-nematic transition [8], fluid-solid transition in systems interacting via the inverse power potential $u(r) = \epsilon(\sigma/r)^n$ where ϵ, σ and n are potential parameters and r is molecular separation [9–11] and freezing of fluids of hard spheres into crystalline and glossy phases [12] are very encouraging. Furthermore, the theory predicts that the fluids interacting via the inverse power potentials freeze into a face-centred-cubic (fcc) lattice when the potential parameter $n \geq 6.5$ and into the body-centred-cubic (bcc) lattice when $n \leq 6$ and the fluid-bcc-fcc triple point is at $1/n = 0.158$ [11]. These results are in very good agreement with simulation results. To best of our knowledge this is the only free energy functional which correctly describes the relative stability of the two cubic phases.

In this paper we apply the theory to investigate freezing of fluids interacting via the 6-12 Lennard-Jones(LJ) potential,

$$u(r) = 4\epsilon \left(\left(\frac{\sigma}{r} \right)^{12} - \left(\frac{\sigma}{r} \right)^6 \right), \quad (1.1)$$

where ϵ and σ are potential parameters, and compare our results with the results found from other free energy functionals as well as with simulation results. Also, in order to estimate the role played by the attractive and repulsive parts of the LJ potential in formation of crystalline structure at the freezing point we consider the purely repulsive Weeks-Chandler-Anderson (WCA) reference potential defined as[13]

$$u_R(r) = \begin{cases} u(r) + \epsilon & \text{for } r \leq r_m \\ 0 & \text{for } r \geq r_m, \end{cases} \quad (1.2)$$

where $r_m(= 2^{1/6}\sigma)$ is the value of r at which the LJ potential has its minimum value. Henceforth, we refer this potential as a reference Lennard-Jones (RLJ) potential. While the LJ potential mimics characteristics of interaction potential of the rare-gas elements and even of some molecular systems, the RLJ potential is used to model interactions in polymers [14] and dendrimers [15]. The freezing parameters for these systems calculated by de Kuijper et al [6] using RY free energy functional (RY-DFT), the modified weighted density approximation (MWDA) [16] and the modified effective liquid approximation (MELA)[17] show that these theories fail to give satisfactory description of the transition.

The paper is organized as follows: In Sec II we give a brief description of the free -energy functional for a crystal that contains both the symmetry conserving and the symmetry broken parts of DPCF. In Sec III we describe calculation of these functions and report results. In Sec IV the freezing parameters are calculated and compared with simulation results as well as with results found from other (approximate) theories. The paper ends with a brief summary and conclusions given in Sec V.

II. THEORY

The formation of a crystalline structure defined by a set of discrete vectors \vec{R} at the freezing point leads to emergence of a qualitatively new contribution in distribution of particles [9–12]. The correlation functions in a crystal can therefore be written as a sum of

two qualitatively different contributions; one that preserves the continuous symmetry of the fluid and one that breaks it and vanishes in the fluid [11]. Thus for the DPCF in a crystal we write

$$c(\vec{r}_1, \vec{r}_2) = c^{(0)}(|\vec{r}_2 - \vec{r}_1|; \rho_s) + c^{(b)}(\vec{r}_1, \vec{r}_2; [\rho]), \quad (2.1)$$

where $c^{(0)}$ and $c^{(b)}$ represent respectively, the symmetry conserving and symmetry broken contributions. Note that $c^{(0)}$ depends on the magnitude of inter-particle separation r and is a function of average crystal density, ρ_s while $c^{(b)}$ is functional of $\rho(\vec{r})$ (indicated by square bracket) depends on position vectors \vec{r}_1 and \vec{r}_2 and is invariant only under a discrete set of translations corresponding to lattice vectors \vec{R} . The DPCF $c(\vec{r}_1, \vec{r}_2)$ is related with the total correlation function $h(\vec{r}_1, \vec{r}_2)$ through the Ornstein - Zernike (OZ) equation [18]. The reduced free energy functional $A[\rho]$ has an ideal gas part,

$$A_{id}[\rho] = \int d\vec{r} \rho(\vec{r}) (\ln \rho(\vec{r}) \Lambda - 1), \quad (2.2)$$

where Λ is cube of thermal wavelength associated with a particle, and the excess part $A_{ex}[\rho]$ arising due to interparticle interactions. This excess part $A_{ex}[\rho]$ is related to $c(\vec{r}_1, \vec{r}_2)$ as [2, 17],

$$\frac{\delta^2 A_{ex}[\rho]}{\delta \rho(r_1) \delta \rho(r_2)} = -c(\vec{r}_1, \vec{r}_2). \quad (2.3)$$

Using Eq(2.1) one can rewrite Eq(2.3) as

$$\frac{\delta^2 A_{ex}^{(0)}[\rho]}{\delta \rho(r_1) \delta \rho(r_2)} = -c^{(0)}(|\vec{r}_2 - \vec{r}_1|; \rho_s), \quad (2.4)$$

$$\frac{\delta^2 A_{ex}^{(b)}[\rho]}{\delta \rho(r_1) \delta \rho(r_2)} = -c^{(b)}(\vec{r}_1, \vec{r}_2; [\rho]), \quad (2.5)$$

where $A_{ex}^{(0)}[\rho] + A_{ex}^{(b)}[\rho] = A_{ex}[\rho]$.

The expressions for $A_{ex}^{(0)}$ and $A_{ex}^{(b)}$ are found from functional integrations of Eqs(2.4) and (2.5), respectively. In this integration the system is taken from some initial density to the

final density distribution along a path in the density space, the result is independent of the path of integration. These integrations give [10, 11],

$$A_{ex}^{(0)}[\rho] = A_{ex}(\rho_l) + \beta\mu - \ln(\rho_l\Lambda) - \frac{1}{2} \int d\vec{r}_1 \int d\vec{r}_2 (\rho(\vec{r}_1) - \rho_l) (\rho(\vec{r}_2) - \rho_l) \bar{c}^{(0)}(|\vec{r}_2 - \vec{r}_1|; \rho_l), \quad (2.6)$$

and

$$A_{ex}^{(b)}[\rho] = -\frac{1}{2} \int d\vec{r}_1 \int d\vec{r}_2 (\rho(\vec{r}_1) - \rho_s) (\rho(\vec{r}_2) - \rho_s) \bar{c}^{(b)}(\vec{r}_1, \vec{r}_2), \quad (2.7)$$

where

$$\bar{c}^{(0)}(|\vec{r}_2 - \vec{r}_1|; \rho_l) = 2 \int_0^1 d\lambda \lambda \int_0^1 d\lambda' c^{(0)}(|\vec{r}_2 - \vec{r}_1|; \rho_l + \lambda\lambda'(\rho_s - \rho_l)), \quad (2.8)$$

$$\bar{c}^{(b)}(\vec{r}_1, \vec{r}_2) = 4 \int_0^1 d\xi \xi \int_0^1 d\xi' \int_0^1 d\lambda \lambda \int_0^1 d\lambda' c^{(b)}(\vec{r}_1, \vec{r}_2; \lambda\lambda'\rho_s; \xi\xi'\rho_G). \quad (2.9)$$

In above equations, $A_{ex}(\rho_l)$ is reduced excess free energy of the coexisting fluid of density ρ_l and chemical potential μ , $\rho_s = \rho_l(1 + \Delta\rho^*)$ is average density of the crystal, $\beta = (k_B T)^{-1}$ is the inverse temperature in unit of the Boltzmann constant k_B . The order parameter ρ_G which appears in the expansion of $\rho(\vec{r})$ in the Fourier series as,

$$\rho(\vec{r}) = \rho_s + \sum_{G \neq 0} \rho_G e^{i\vec{G} \cdot \vec{r}}, \quad (2.10)$$

is amplitude of density wave of wavelength equal to $2\pi/|\vec{G}|$ where \vec{G} is reciprocal lattice vector (RLV). The summation in Eq(2.10) is over the complete set of RLV of a given crystal.

The free energy functional $A[\rho]$ for a crystal is sum of A_{id} , $A_{ex}^{(0)}$ and $A_{ex}^{(b)}$. Thus

$$\begin{aligned} A[\rho] = & \int d\vec{r} \rho(\vec{r}) (\ln(\rho(\vec{r})\Lambda) - 1) + A_{ex}(\rho_l) + [\beta\mu - \ln(\rho_l\Lambda)] \int d\vec{r} (\rho(\vec{r}) - \rho_l) \\ & - \frac{1}{2} \int d\vec{r}_1 \int d\vec{r}_2 (\rho(\vec{r}_1) - \rho_l) (\rho(\vec{r}_2) - \rho_l) \bar{c}^{(0)}(|\vec{r}_2 - \vec{r}_1|; \rho_l) \\ & - \frac{1}{2} \int d\vec{r}_1 \int d\vec{r}_2 (\rho(\vec{r}_1) - \rho_s) (\rho(\vec{r}_2) - \rho_s) \bar{c}^{(b)}(\vec{r}_1, \vec{r}_2). \end{aligned} \quad (2.11)$$

This expression of $A[\rho]$ which includes both the symmetry conserving and symmetry broken contributions of the DPCF is exact; no approximation has been used in deriving it. In the RY free energy functional the contribution arising due to $c^{(b)}$ was neglected.

In locating the freezing transition, the grand thermodynamic potential defined as

$$-W = A - \beta\mu \int d\vec{r}\rho(\vec{r}) \quad (2.12)$$

is generally used as it ensures that the pressure and the chemical potential μ of the two phases remain equal at the transition. The fluid-solid coexistence is obtained when $\Delta W = W_l - W = 0$, where W_l is the grand thermodynamic potential of the coexisting fluid, and $\delta W/\delta\rho(r) = 0$ are simultaneously satisfied.

The expression for ΔW is found to be [10, 11]

$$\begin{aligned} \Delta W = & \int d\vec{r} \left[\rho(\vec{r}) \ln \left(\frac{\rho(\vec{r})}{\rho_l} \right) - (\rho(\vec{r}) - \rho_l) \right] \\ & - \frac{1}{2} \int d\vec{r}_1 \int d\vec{r}_2 (\rho(\vec{r}_1) - \rho_l) (\rho(\vec{r}_2) - \rho_l) \bar{c}^{(0)}(|\vec{r}_2 - \vec{r}_1|) \\ & - \frac{1}{2} \int d\vec{r}_1 \int d\vec{r}_2 (\rho(\vec{r}_1) - \rho_l) (\rho(\vec{r}_2) - \rho_l) \bar{c}^{(b)}(\vec{r}_1, \vec{r}_2) \end{aligned} \quad (2.13)$$

The minimisation is done with an assumed form of $\rho(\vec{r})$. The ideal part is calculated using a form for $\rho(\vec{r})$ which is a superposition of normalised Gaussians centred around the lattice site,

$$\rho(\vec{r}) = \left(\frac{\alpha}{\pi} \right)^{3/2} \sum_n \exp \left[-\alpha \left(\vec{r} - \vec{R}_i \right)^2 \right], \quad (2.14)$$

where α is the localization parameter. For the interaction part it is convenient to use Eq(2.10). The order parameter $\rho_G = \rho\mu_G$ that appears in Eq(2.10) is related to parameter α ;

$$\mu_G = \exp \left[-\frac{G^2}{4\alpha} \right]$$

III. CALCULATION OF $c^{(0)}(r)$ AND $c^{(b)}(r_1, r_2)$

A. Calculation of $c^{(0)}(r)$, $h^{(0)}(r)$ and their derivative with respect to ρ

The values of pair correlation functions $h^{(0)}$ and $c^{(0)}$ are found from simultaneous solution of the OZ equation,

$$h^{(0)}(r) = c^{(0)}(r) + \rho \int d\vec{r}' c^{(0)}(r') h^{(0)}(|\vec{r}' - \vec{r}|), \quad (3.1)$$

and a closure relation that relates pair correlation functions to pair potential. We use the HMSA (hybridized-mean-spherical approximation) closure of Zerah and Hansen(ZH) [19] which interpolates between the hyper-netted chain (HNC) and soft-core mean spherical approximation (SMSA) relation via a continuous mixing function. The ZH relation is written as

$$1 + h^{(0)}(r) = \exp[-\beta u_0(r)] \ln \left[1 + \frac{\exp(f(r)(\chi^{(0)}(r) - \beta u_p(r))) - 1}{f(r)} \right], \quad (3.2)$$

where $\chi^{(0)}(r) = h^{(0)}(r) - c^{(0)}(r)$, $f(r)$ is the mixing parameter and $u_0(r)$ and $u_p(r)$ are suitably chosen short-range part and long ranged part of pair potential $u(r)$. The function $f(r) = 1 - \exp(-\psi(r))$ includes an adjustable parameter ψ which value is chosen to satisfy thermodynamic self consistency between the virial and compressibility routes of the equation of state. This requirement gave us values of $f(r)$ which are in agreement with those reported in ref. [19] for both systems.

We used the following two schemes for division of $u(r)$ of Eq(1.1) into $u_0(r)$ and $u_p(r)$. In the WCA scheme (WCAS) $u_0(r)$ is the RLJ potential of Eq(1.2) and

$$u_p(r) = \begin{cases} -\epsilon & r < r_m (= 2^{1/6}\sigma) \\ u(r) & r > r_m, \end{cases} \quad (3.3)$$

In the other scheme referred to as optimized division scheme (ODS) [20] $u_p(r)$ is written as

$$u_p(r) = \begin{cases} -p\epsilon & r \leq r_1 \\ a_1 + a_2r + a_3r^2 + a_4r^3 & r_1 < r \leq r_2 \\ u(r) & r > r_2 \end{cases} \quad (3.4)$$

and $u_0(r) = u(r) - u_p(r)$. Note that for $p = 1$ and $r_1 = r_2$ the ODS reduces to the WCAS.

The values of a_i parameters are

$$\begin{aligned} a_1 &= \frac{r_1^3 u(r_2) - r_1^3 r_2 u'(r_2) - 3r_1^2 r_2 u(r_2) + r_1^2 r_2^2 u'(r_2) + 3p\epsilon r_1 r_2^2 - p\epsilon r_2^3}{(r_1 - r_2)^3}, \\ a_2 &= -\frac{r_1(-r_1^2 u'(r_2) - r_1 r_2 u'(r_2) + 6p\epsilon r_2 - 6r_1 u(r_2) + 2r_2^2 u'(r_2))}{(r_1 - r_2)^3}, \\ a_3 &= \frac{-2r_1^2 u'(r_2) + 3p\epsilon r_1 - 3r_1 u(r_2) + r_1 r_2 u'(r_2) + 3p\epsilon r_2 - 3r_2 u(r_2) + r_2^2 u'(r_2)}{(r_1 - r_2)^3}, \\ a_4 &= -\frac{-r_1 u'(r_2) - 2u(r_2) + r_2 u'(r_2) + 2p\epsilon}{(r_1 - r_2)^3}, \end{aligned} \quad (3.5)$$

with $p = 2$, $r_1 = 0.88\sigma$, $r_2 = 1.6\sigma$ and $u'(r) = \frac{\partial u(r)}{\partial r}$.

For RLJ potential $u_p(r)$ is zero and the ZH closure reduces to the of Roger and Young closure [21].

The OZ and closure relations for $\frac{\partial h^{(0)}(r)}{\partial \rho}$ and $\frac{\partial c^{(0)}(r)}{\partial \rho}$ are found by differentiating Eqs(3.1) and (3.2) with respect to ρ . Thus

$$\begin{aligned} \frac{\partial \chi^{(0)}(r)}{\partial \rho} &= \int d\vec{r}' c^{(0)}(r') h^{(0)}(|\vec{r}' - \vec{r}|) \\ &\quad + \rho \int d\vec{r}' \frac{\partial c^{(0)}(r')}{\partial \rho} h^{(0)}(|\vec{r}' - \vec{r}|) \\ &\quad + \rho \int d\vec{r}' c^{(0)}(r') \frac{\partial h^{(0)}(|\vec{r}' - \vec{r}|)}{\partial \rho} \end{aligned} \quad (3.6)$$

and

$$\frac{\partial h^{(0)}(r)}{\partial \rho} = e^{-\beta u_0(r)} \frac{\partial \chi^{(0)}(r)}{\partial \rho} e^{f(r)(\chi^{(0)}(r) - \beta u_p(r))} \quad (3.7)$$

The closed set of coupled equations (3.1),(3.2)and (3.6)-(3.7)have been solved for four unknowns $h^{(0)}(r)$, $c^{(0)}(r)$, $\frac{\partial h^{(0)}(r)}{\partial \rho}$ and $\frac{\partial c^{(0)}(r)}{\partial \rho}$ for potentials of Eqs(1.1) and (1.2).

In Fig.1 we compare $g^{(0)}(r) = 1 + h^{(0)}(r)$ found from WCAS and ODS of division of LJ potential with simulation results[22] for ρ^* ($= \rho\sigma^3$) = 0.4 and 0.9 at T^* ($= k_B T/\epsilon$) = 1.5. As found in ref. [20] the ODS gives better agreement particularly at the first maximum with simulation results than the WCAS. In Fig.2 we compare $\hat{c}^{(0)}(q)$ (the Fourier transform of $c^{(0)}(r)$) found from these two schemes for $\rho^* = 1.05$ at $T^* = 1.50$ and $\rho^* = 1.50$ at $T^* = 10.0$ which are close to freezing point. On the scale of the figure the two schemes give almost same values of $\hat{c}^{(0)}(q)$ except at small value of q . In Table-I we compare values of $\hat{c}^{(0)}(G)$ where $G = \frac{2\pi}{a}\sqrt{l^2 + m^2 + n^2}$ (l, m, n being integers) are RLV of a fcc lattice and $a = (4/\rho^*)^{1/3}$ for $\rho^* = 1.074$ at $T^* = 1.50$ and $\rho^* = 1.556$ at $T^* = 10.0$ found from the two schemes. Though the difference in the values of $\hat{c}(G)$ is small, it has noticeable effect on the freezing parameters as shown below in Figs 9 and 10 and Table-III. In Fig.3 we compare values of $g^{(0)}(r)$ of LJ potential with that of RLJ potential at $\rho^* = 0.4$ and 0.9 for $T^* = 1.50$. The two values are in good agreement at high density but differ at lower density; this is because of the contribution of attractive interaction which decreases with increasing density.

B. Calculation of $c^b(\vec{r}_1, \vec{r}_2)$

One can use the relation

$$\frac{\delta^{n-2}c(\vec{r}_1, \vec{r}_2)}{\delta\rho(\vec{r}_3)\cdots\delta\rho(\vec{r}_n)} = c_n(\vec{r}_1, \vec{r}_2, \cdots, \vec{r}_n), \quad (3.8)$$

where c_n is the n-body direct correlation function (DPF) and the functional Taylor expansion to write the following series for $c^b(\vec{r}_1, \vec{r}_2)$.

$$\begin{aligned} c^{(b)}(\vec{r}_1, \vec{r}_2) &= \int d\vec{r}_3 c_3^{(0)}(\vec{r}_1, \vec{r}_2, \vec{r}_3; \rho_s)(\rho(\vec{r}_3) - \rho_s) \\ &\quad + \frac{1}{2} \int d\vec{r}_4 c_4^{(0)}(\vec{r}_1, \vec{r}_2, \vec{r}_3, \vec{r}_4; \rho_s)(\rho(\vec{r}_3) - \rho_s)(\rho(\vec{r}_4) - \rho_s) \\ &\quad + \cdots \end{aligned} \quad (3.9)$$

In Eq(3.9) $c_m^{(0)}$ is the m-body DCF of a homogeneous system of density ρ_s and $\rho(\vec{r}) - \rho_s = \sum_G \rho_G \exp(i\vec{G} \cdot \vec{r})$. The values of $c_m^{(0)}$ can be found from exact relations

$$\frac{\partial^n c^{(0)}(r; \rho)}{\partial \rho^n} = \int d\vec{r}_3 \cdots \int d\vec{r}_n c_{n+2}^{(0)}(\vec{r}_1, \vec{r}_2, \dots, \vec{r}_{n+2}). \quad (3.10)$$

The values of $\frac{\partial^n c^{(0)}(r; \rho)}{\partial \rho^n}$ and the factorization *ansatz* can be used to find values of $c_{n+2}^{(0)}$ from Eq(3.10). The factorization *ansatz* which was first used by Barrat et al [23] to calculate $c_3^{(0)}$ has recently been extended by Bharadwaj et al [11] to calculate $c_4^{(0)}$.

In the case of inverse power potential it was found that at the melting point $c^{(b)}$ is accurately approximated by the first term of series (3.9) even for very soft repulsions[11]; the contribution made by $c^{(b)}$ to free energy increases with the range of the potential. Since, as shown below, the contribution made by the attractive part of the LJ potential at the transition point is small and contribute opposite to that of the repulsive part, we expect the conclusion drawn in case of the inverse power potentials holds in the present systems as well. In view of this, we consider the first term of series (3.9) and examine its effect on the freezing parameters. Following Barrat et al [23] we write

$$c_3^{(0)}(\vec{r}_1, \vec{r}_2, \vec{r}_3) = t(r_{12})t(r_{13})t(r_{23}) \quad (3.11)$$

and determine the function $t(r)$ from the relation

$$\frac{\partial c^{(0)}(r; \rho)}{\partial \rho} = t(r) \int d\vec{r}' t(r') t(|\vec{r}' - \vec{r}|) \quad (3.12)$$

using an iterative procedure. From known values of $t(r)$, $c_3^{(0)}$ is found from Eq(3.11). It was shown in ref [23] that the value of $c_3^{(0)}$ calculated in this way for the inverse power potential agrees with simulation results. It may also be shown that $\hat{c}^{(0)}(\vec{q}_1, \vec{q}_2, \vec{q}_3)$ agrees with exact three-body DCF at least up to the second order in the wave numbers.

Using Eq(3.11) in the first term of the series (3.9) and substituting the value of $\rho(\vec{r}_3) - \rho_s$ we find

$$c^{(b)}(\vec{r}_1, \vec{r}_2) = \sum_G e^{i\vec{G}\cdot\vec{r}_c} t(r) e^{-\frac{1}{2}i\vec{G}\cdot\vec{r}} \int d\vec{r}' t(r') t(|\vec{r}' - \vec{r}|) e^{i\vec{G}\cdot\vec{r}'} \quad (3.13)$$

where $\vec{r} = \vec{r}_2 - \vec{r}_1$, $\vec{r}_c = \frac{1}{2}(\vec{r}_1 + \vec{r}_2)$ and $\vec{r}' = \vec{r}_3 - \vec{r}_1$

This is solved to give [9, 11, 12]

$$c^{(b)}(\vec{r}_1, \vec{r}_2) = \sum_G e^{i\vec{G}\cdot\vec{r}_c} \sum_{lm} c_l^{(G)}(r) Y_{lm}^*(\hat{G}) Y_{lm}(\hat{r}) \quad (3.14)$$

where

$$c_l^{(G)}(r) = \rho_G \sum_{l_1} \sum_{l_2} \Lambda(l, l_1, l_2) j_{l_2} \left(\frac{1}{2} Gr \right) B_{l_1}(r, G) \quad (3.15)$$

Here $j_l(x)$ is the spherical Bessel function, $Y_{lm}(\hat{x})$ the spherical harmonics,

$$\Lambda(l, l_1, l_2) = (i)^{l_1+l_2} (-1)^{l_2} \left[\frac{(2l_1+1)(2l_2+1)}{2l+1} \right] [C_g(l_1, l_2, l; 0, 0, 0)]^2$$

and

$$B_{l_1}(r, G) = 8 t(r) \int dk k^2 t(k) j_{l_1}(kr) \int dr' r'^2 t(r') j_{l_1}(kr') j_{l_1}(Gr')$$

where C_g is the Clebsh-Gardon coefficient. The crystal symmetry dictates that l and $l_1 + l_2$ are even and for cubic crystal $m = 0, \pm 4$.

The values of $c_l^{(G)}(r)$ depend on order parameters μ_G and on magnitude of \vec{G} . In Figs 4-6 we plot and compare $\frac{c_l^{(G)}(r)}{\mu_G}$ for $l = 0, 2, 4$ and 6 for RLV's of first three sets, respectively, of a fcc lattice at $\rho_s^* = 1.10$ and $T^* = 1.50$; the full and dashed lines correspond to LJ (found using WCAS) and RLJ potentials respectively. For a different set of RLV's $\frac{c_l^{(G)}(r)}{\mu_G}$ varies with r in different ways. The values in all cases become negligible for r (r is measured in unit of σ) > 2.5 . For any given G , $\frac{c_l^{(G)}(r)}{\mu_G}$ decreases rapidly with l ; major contribution comes from $l = 0$ and 2. For $l = 6$ the value is about three order of magnitude smaller than that of $l = 0$. It is also seen that at any given point r , values of $\frac{c_l^{(G)}(r)}{\mu_G}$ are positive for some set of G while for other values are negative, leading to mutual cancellation in a quantity where summation over G is involved. The difference between the values of $\frac{c_l^{(G)}(r)}{\mu_G}$ of LJ and RLJ is maximum for the first set of \vec{G} vectors and becomes almost negligible for other sets, showing the limited effect that the attractive interaction has on crystal structure.

C. Calculation of $\bar{c}^{(0)}(r)$ and $\bar{c}^{(b)}(\vec{r}_1, \vec{r}_2)$

As shown in ref [10, 11], $\bar{c}^{(0)}(r; \rho)$ can be approximated as

$$\bar{c}^{(0)}(r; \rho) = c^{(0)}(r; \rho_l) + \frac{1}{3} \rho_l \Delta \rho^* \frac{\partial c^{(0)}(r; \rho_l)}{\partial \rho_l}$$

where the contribution arising from the second term to the free energy is found to be negligibly small and one can replace $\bar{c}^{(0)}(r; \rho)$ by $c^{(0)}(r; \rho_l)$.

For evaluation of $\bar{c}^{(b)}$, we note that it is linear in order parameter and the integration over ξ variable in Eq(2.9) can be performed analytically leading to

$$\bar{c}^{(b)}(\vec{r}_1, \vec{r}_2) = \sum_G e^{i\vec{G} \cdot \vec{r}_c} \sum_{lm} \bar{c}_l^{(G)}(r) Y_{lm}^*(\hat{G}) Y_{lm}(\hat{r})$$

where

$$\bar{c}_l^{(G)}(r) = \rho_G \sum_{l_1} \sum_{l_2} \Lambda(l, l_1, l_2) j_{l_2} \left(\frac{1}{2} Gr \right) \bar{B}_{l_1}(r, G)$$

with

$$\bar{B}_{l_1}(r, G) = 2 \int_0^1 d\lambda (1 - \lambda) B_{l_1}(r, G; \lambda \rho)$$

The quantity $B_{l_1}(r, G)$ is defined by Eq(3.15). The integration over λ has been performed numerically by varying it from 0 to 1 on a fine grid and evaluating B_{l_1} on these densities. Since this function vary smoothly with density and its value has been evaluated at closely spaced values of density, the result for $\bar{c}^{(b)}(\vec{r}_1, \vec{r}_2)$ is expected to be accurate.

As noted in ref [6], the HMSA closure dose not give self-consistent solutions for these potentials at low densities and low temperatures ($\rho^* \leq 0.5$ and $T^* \leq 1.0$) we could not calculate accurately the value of $\bar{c}^{(b)}(\vec{r}_1, \vec{r}_2)$ below the critical temperature ($T_c^* \simeq 1.35$) for the LJ potential and for $T^* \leq 1$ for the RLJ potential. Below these temperatures we have therefore used extrapolated values of free energy contribution due to symmetry broken part of DPCF (see Fig 11) to locate the freezing transition.

IV. LIQUID-SOLID TRANSITION

From Eqs (2.12)-(2.13) and expressions for $\bar{c}^{(0)}(r)$ and $\bar{c}^{(b)}(\vec{r}_1, \vec{r}_2)$ given above one finds [9, 11, 12]

$$\frac{\Delta W}{N} = \frac{\Delta W_{id}}{N} + \frac{\Delta W_0}{N} + \frac{\Delta W_b}{N} \quad (4.1)$$

where

$$\frac{\Delta W_{id}}{N} = 1 - (1 + \Delta\rho^*) \left[\frac{5}{2} + \ln\rho_l^* - \frac{3}{2} \ln\left(\frac{\alpha}{\pi}\right) \right], \quad (4.2)$$

$$\frac{\Delta W_0}{N} = -\frac{1}{2} \rho_l^* \Delta\rho^{*2} \bar{c}^{(0)}(0) - \frac{1}{2} \rho_l^* (1 + \Delta\rho^*)^2 \sum_{G \neq 0} |\mu_G|^2 \bar{c}^{(0)}(G), \quad (4.3)$$

$$\frac{\Delta W_b}{N} = -\frac{1}{2} \rho_l^* (1 + \Delta\rho^*)^2 \sum_G' \sum_{G_1}' \mu_{G_1} \mu_{-G-G_1} \bar{c}^{(G)} \left(\vec{G}_1 + \frac{1}{2} \vec{G} \right) \quad (4.4)$$

Here ΔW_{id} , ΔW_0 and ΔW_b are respectively, the ideal, the symmetry-conserving and the symmetry broken contributions to ΔW . The prime on summation in Eq(4.4) indicates the condition $\vec{G} \neq 0$, $\vec{G}_1 \neq 0$ and $\vec{G}_1 \neq \vec{G}$ and

$$\hat{c}^{(0)}(G) = 4\pi \int dr r^2 c^{(0)}(r) j_0(Gr), \quad (4.5)$$

$$\hat{c}^{(G)}(\vec{A}) = 4\pi \sum_{lm} i^l \int dr r^2 c_l^{(G)}(r) j_l(Ar) Y_{lm}(\hat{A}), \quad (4.6)$$

where $\vec{A} = \left(\vec{G}_1 + \frac{1}{2} \vec{G} \right)$.

These equations are used to locate the fluid-fcc crystal transition. The reason for selecting the fcc structure are following; (i) these systems are known to freeze into fcc crystal, (ii) simulation data are mostly for fluid-fcc crystal transition [24–29] and (iii) the difference between freezing density of fcc lattice and hexagonal closed packed (hcp) lattice is very small (the hcp density is slightly higher). The $\frac{\Delta W}{N}$ is minimized with respect to two parameters ρ_s^* and α . For a given ρ_s^* and $\Delta\rho^*$, $\frac{\Delta W}{N}$ is minimised with respect to α ; next $\Delta\rho^*$ is varied till the lowest value of $\frac{\Delta W}{N}$ at its minimum is found. If this lowest value of $\frac{\Delta W}{N}$ is not zero then ρ_s^* is varied until $\frac{\Delta W}{N}$ is zero. The lowest value of ρ_s^* and corresponding $\rho_l^* = \rho_s^*/(1 + \Delta\rho^*)$ for which the condition $\frac{\Delta W}{N} = 0$ is satisfied are taken as the coexisting solid and fluid densities at the transition. This procedure has been used in finding values of freezing parameters from the present theory (Eqs (4.1) - (4.6)) as well as from the RY-DFT.

In Table-II we compare values of freezing parameters ρ_l^* , ρ_s^* , $\Delta\rho^*$, the Lindemann parameter L and $P^* = P\sigma^3/\epsilon$, where P is the pressure at the freezing point, found from our theory with those found from the RY-DFT, MWDA [6] and simulations [28, 29] for the RLJ potential. The RY-DFT gives values of ρ_l^* and P^* which are quite high compared to simulation values, e.g. at $T^* = 2$, ρ_l^* is about 9% and P^* is about 34% higher. The MWDA while gives relatively better agreement at higher temperatures, fails at low temperatures. The values found from our theory, (given in the first row of the table) are in very good agreement with simulation results for the entire temperature range.

In Fig.7 we plot the solid - fluid phase diagram; the lines (full line for fcc crystal and dashed line for fluid) are from the present theory and circles and squares (open for fluid and full for crystal) are from simulations [28, 29]. We note large spread in simulation values. This may be due to different theoretical methods used in locating the transition and system sizes in the calculation. One may also note the values given in ref [28] for low temperatures ($T^* \leq 2.74$) and high temperatures ($T^* \geq 3.63636$) do not seem to join smoothly. This may be due to use of two different algorithms in these two temperature regions. In Fig.8 we plot P^* vs T^* , dashed line from present theory, full line from RY-DFT and open circles and triangles from simulations and squares from MWDA.

In Table-III we compare the values of freezing parameters for the LJ potential. The values found from ODS and WCAS of division of potential into reference and perturbation are also compared. It may be noted that while the values of ρ_l^* , ρ_s^* and therefore P^* found from ODS are somewhat higher but $\Delta\rho^*$ is lower than those found from WCAS, This is because of the difference in the values of $\hat{c}(q)$ shown in Fig.2 and Table-I. As in the case of RLJ potential, the values found from RY-DFT for ρ_l^* , ρ_s^* and P^* are quite high compared to simulation values. The MWDA, as shown in ref. [6] did not yield a (meta-) stable solid phase at $T^* < 5.00$. However, at $T^* = 10.0$ the theory gave values which are in good agreement with simulation results.

The solid-fluid phase diagram is plotted in Fig.9. The simulation values given in the table and in the figure are of Agrawal and Kofke [24], Ahmed and Sadus [25], Sousa *et al.* [26] and Hansen and Verlet [27], Hansen [27]. The large spread in the simulation values is seen in this case also. While both the ODS and WCAS results are in good agreement with simulation results, the ODS values are in better agreement with simulation values at high temperatures $T^* > 2.0$ whereas WCAS values are closer to simulation values for $T^* < 2.0$. The value of

Lindemann parameter (a measure of the relative displacement of particle around its lattice position) found by both methods is almost same and varies marginally with temperature; e.g. it varies from 0.092 at $T^* = 0.8$ to 0.107 at $T^* = 10.0$. In Fig.10 P^* and T^* is plotted and compared with simulation and RY-DFT results.

V. SUMMERY AND CONCLUSIONS

The free energy functional proposed by Singh and Singh [9] for a crystal is used to calculate freezing parameters of simple systems interacting via the LJ and the RLJ potentials. This free energy functional is exact and involves the symmetry conserving part of the DPCF, $c^{(0)}(r, \rho)$ and the symmetry broken part, $c^{(b)}(\vec{r}_1, \vec{r}_2)$ as input informations. The values of $c^{(0)}(r)$ which corresponds to isotropy and homogeneity of the phase are found from the integral equation theory comprising the OZ equation and the ZH closure relation[19]. For $c^{(b)}(\vec{r}_1, \vec{r}_2)$, which is a functional of $\rho(\vec{r})$ and is invariant only under a discrete set of translations and rotations, an expansion in ascending powers of order parameters has been used. This expansion involves higher body direct correlation functions of isotropic systems at average density of the crystal ρ_s , which in turn were found from the density derivatives of $c^{(0)}(r)$ using a method describe in refs.[9–12].

Through the contribution of symmetry broken part of DPCF to the grand thermodynamic potential is small compared to the symmetry conserving part, it plays crucial role in freezing of fluids. In Table-IV we compare the contribution made by the ideal gas part, $\frac{\Delta W_{id}}{N}$, the symmetry conserving part, $\frac{\Delta W_0}{N}$, and the symmetry broken part, $\frac{\Delta W_b}{N}$ at the freezing point for both potentials at different temperatures. As $\frac{\Delta W_b}{N}$ is negative it adds to $\frac{\Delta W_0}{N}$ to overcome the positive contribution of $\frac{\Delta W_{id}}{N}$ in order to make $\frac{\Delta W}{N} = 0$. We note that the contribution of $\frac{\Delta W_b}{N}$, compared to $\frac{\Delta W_0}{N}$, increases with the temperature; albeit marginally. For example it increases from 12.6% at $T^* = 0.8$ to 16.0% at $T^* = 10.0$ for RLJ potential and from 11.0% at $T^* = 0.8$ to 15.3% at $T^* = 10.0$ for the LJ potential. We also note that at the same temperature the relative contribution of $\frac{\Delta W_b}{N}$ for LJ potential is marginally lower than that for RLJ potential. In Fig-11 the values of $\frac{\Delta W_0}{N}$ and $\frac{\Delta W_b}{N}$ at the freezing point for these two potentials as a function of temperature are compared. One may note that while attractive interaction contribution to $\frac{\Delta W_0}{N}$ is to increase its value, it decreases the value of $\frac{\Delta W_b}{N}$. This shows that the contribution of attractive interaction to $\frac{\Delta W_b}{N}$ is small and opposite to that

of repulsive potential part of interaction. However, these contributions are small leading to conclusion that freezing is predominately determined by the repulsive part of the interaction.

The difference in the values of freezing parameters for the LJ potential found from ODS and WCAS shows that the value of freezing parameters are sensitive to values of DPCF.

In conclusion, we wish to emphasize that the agreement between theory and simulation values of freezing parameters for potentials studied here and elsewhere[9–12] shows that the free energy functional proposed by Singh and Singh[9] provides an accurate theory for fluid - solid transition for a wide class of potentials. As this free energy functional takes into account the spontaneous symmetry breaking, it can be used to study solid-solid transitions as well as other properties of crystals.

ACKNOWLEDGEMENTS

We are thankful to the Department of Science and Technology (DST), University Grants Commission (UGC) and Indian National Science Academy for financial support.

-
- [1] T. V. Ramakrishnan and M. Yussouff, *Phys. Rev. B* **19**, 2775 (1979).
 - [2] A. D. J. Haymet and D. W. Oxtoby, *The Journal of Chemical Physics* **74**, 2559 (1981).
 - [3] Y. Singh, *Physics Reports* **207**, 351 (1991).
 - [4] P. Tarazona, *Phys. Rev. A* **31**, 2672 (1985).
 - [5] W. A. Curtin and N. W. Ashcroft, *Phys. Rev. A* **32**, 2909 (1985).
 - [6] A. de Kuijper, W. L. Vos, J.-L. Barrat, J.-P. Hansen, and J. A. Schouten, *The Journal of Chemical Physics* **93**, 5187 (1990).
 - [7] D. C. Wang and A. P. Gast, *The Journal of Chemical Physics* **110**, 2522 (1999).
 - [8] P. Mishra and Y. Singh, *Phys. Rev. Lett.* **97**, 177801 (2006); P. Mishra, S. L. Singh, J. Ram, and Y. Singh, *The Journal of Chemical Physics* **127**, 044905 (2007).
 - [9] S. L. Singh and Y. Singh, *EPL (Europhysics Letters)* **88**, 16005 (2009).
 - [10] A. Jaiswal, S. L. Singh, and Y. Singh, *Phys. Rev. E* **87**, 012309 (2013).
 - [11] A. S. Bharadwaj, S. L. Singh, and Y. Singh, *Phys. Rev. E* **88**, 022112 (2013).
 - [12] S. L. Singh, A. S. Bharadwaj, and Y. Singh, *Phys. Rev. E* **83**, 051506 (2011).

- [13] J. D. Weeks, D. Chandler, and H. C. Andersen, *The Journal of Chemical Physics* **54**, 5237 (1971).
- [14] M. Kröger, *Physics Reports* **390**, 453 (2004).
- [15] J. T. Bosko, B. D. Todd, and R. J. Sadus, *The Journal of Chemical Physics* **121**, 1091 (2004); *The Journal of Chemical Physics* **124**, 044910 (2006).
- [16] A. R. Denton and N. W. Ashcroft, *Phys. Rev. A* **39**, 4701 (1989).
- [17] M. Baus, *Journal of Physics: Condensed Matter* **1**, 3131 (1989).
- [18] J. Hansen and I. McDonald, *Theory of Simple Liquids (Third Edition)*, third edition ed. (Academic Press, Burlington, 2006).
- [19] G. Zerah and J. Hansen, *The Journal of Chemical Physics* **84**, 2336 (1986).
- [20] J. M. Bomont and J. L. Bretonnet, *The Journal of Chemical Physics* **114**, 4141 (2001).
- [21] F. J. Rogers and D. A. Young, *Phys. Rev. A* **30**, 999 (1984).
- [22] M. Llano-Restrepo and W. G. Chapman, *The Journal of Chemical Physics* **97**, 2046 (1992).
- [23] J.-L. Barrat, J.-P. Hansen, and G. Pastore, *Molecular Physics* **63**, 747 (1988).
- [24] R. Agrawal and D. A. Kofke, *Molecular Physics* **85**, 43 (1995).
- [25] A. Ahmed and R. J. Sadus, *The Journal of Chemical Physics* **131**, 174504 (2009).
- [26] J. M. G. Sousa, A. L. Ferreira, and M. A. Barroso, *The Journal of Chemical Physics* **136**, 174502 (2012).
- [27] J.-P. Hansen and L. Verlet, *Phys. Rev.* **184**, 151 (1969); J.-P. Hansen, *Phys. Rev. A* **2**, 221 (1970).
- [28] A. Ahmed and R. J. Sadus, *Phys. Rev. E* **80**, 061101 (2009).
- [29] A. de Kuijper, J. A. Schouten, and J. P. J. Michels, *The Journal of Chemical Physics* **93**, 3515 (1990).

TABLE I. Comparison of values of $\hat{c}(|\vec{G}|)$ where $|\vec{G}| = \frac{2\pi}{a}\sqrt{l^2 + m^2 + n^2}$ (l, m, n being integers) are RLV of a fcc lattice and $a = (4/\rho^*)^{1/3}$ found from ODS and WCAS of division of the LJ potential at $T^* = 1.50, \rho^* = 1.05$ and $T^* = 10.0, \rho^* = 1.50$.

S.N.	$T^* = 1.50, \rho^* = 1.05$ and $a = 1.55$			$T^* = 10.0, \rho^* = 1.50$ and $a = 1.37$		
	$ \vec{G} $	ODS	WCAS	$ \vec{G} $	ODS	WCAS
0	0.000	-52.40	-48.24	0.000	-39.45	-38.66
1	7.021	0.637	0.632	7.944	0.435	0.436
2	8.107	0.144	0.160	9.173	0.102	0.104
3	11.466	-0.204	-0.225	12.972	-0.128	-0.134
4	13.445	0.253	0.267	15.211	0.163	0.170
5	14.042	0.168	0.174	15.887	0.108	0.112
6	16.215	-0.204	-0.221	18.345	-0.123	-0.129
7	17.669	-0.067	-0.064	19.991	-0.041	-0.040
8	18.129	0.002	0.010	20.510	0.000	0.002
9	19.859	0.106	0.111	22.468	0.063	0.066
10	21.064	0.006	-0.001	23.831	0.007	0.004
11	22.931	-0.077	-0.082	25.944	-0.044	-0.045
12	23.982	-0.029	-0.026	27.133	-0.019	-0.018
13	24.322	-0.008	-0.002	27.518	-0.007	-0.005
14	25.638	0.049	0.055	29.006	0.026	0.028
15	26.582	0.039	0.039	30.074	0.023	0.023

TABLE II: Comparison of freezing parameters $\rho_l^*, \rho_s^*, \Delta\rho^*$, Lindemann parameter L and pressure $P^* = P\sigma^3/\epsilon$ found from the present theory with simulations[28, 29] and with the RY-DFT and the MWDA[6] for the RLJ potential at several values of T^* .

T^*	Simulation/Theory Group	ρ_l^*	ρ_s^*	$\Delta\rho^*$	L	$P\sigma^3/\epsilon$
0.80	Present result	0.930	0.988	0.062	0.092	9.68

Continued on next page

TABLE II – *Continued from previous page*

T^*	Simulation/Theory Group	ρ_l^*	ρ_s^*	$\Delta\rho^*$	L	$P\sigma^3/\epsilon$
	Ry-DFT	0.988	1.058	0.070	0.077	12.48
	MC Simulation [28]	0.920	0.990	0.076		9.60
	MC Simulation* [29]	0.935	1.009	0.079		10.27
1.00	Present result	0.957	1.016	0.061	0.093	12.52
	Ry-DFT	1.022	1.093	0.069	0.076	16.43
	MWDA Theory [6]	0.905	1.015	0.120	0.103	10.40
	MC Simulation [28]	0.950	1.016	0.069		12.57
	MC Simulation [29]	0.952	1.023	0.075		12.60
1.35	Present result	1.002	1.059	0.056	0.094	18.07
	Ry-DFT	1.076	1.147	0.066	0.075	24.17
	MC Simulation* [28]	1.016	1.086	0.069		19.46
	MC Simulation* [29]	0.988	1.056	0.069		17.70
1.50	Present result	1.019	1.075	0.055	0.095	20.52
	Ry-DFT	1.095	1.167	0.066	0.076	27.57
	MC Simulation* [28]	1.034	1.104	0.067		22.11
	MC Simulation [29]	1.010	1.080	0.069		20.60
2.00	Present result	1.066	1.125	0.055	0.096	28.95
	Ry-DFT	1.160	1.231	0.061	0.077	40.83
	MWDA Theory [6]	1.050	1.130	0.080	0.110	27.30
	MC Simulation [28]	1.070	1.140	0.065		30.40
	MC Simulation [29]	1.087	1.159	0.066		32.30
2.74	Present result	1.128	1.187	0.052	0.098	42.91
	Ry-DFT	1.236	1.311	0.060	0.077	62.23
	MC Simulation [28]	1.130	1.200	0.062		45.10
	MC Simulation* [29]	1.176	1.248	0.061		50.41
4.00	Present result	1.214	1.274	0.049	0.100	69.40
	Ry-DFT	1.346	1.421	0.056	0.078	105.14
	MC Simulation* [28]	1.192	1.245	0.045		75.53
	MC Simulation* [29]	1.264	1.333	0.055		80.71
5.00	Present result	1.271	1.331	0.047	0.101	92.49
	Ry-DFT	1.416	1.494	0.055	0.077	142.8
	MWDA Theory [6]	1.275	1.350	0.060	0.110	93.90
	MC Simulation* [28]	1.260	1.317	0.045		102.1
	MC Simulation [29]	1.304	1.370	0.051		104.5
10.00	Present result	1.478	1.539	0.041	0.107	227.8
	Ry-DFT	1.671	1.758	0.052	0.077	369.7
	MC Simulation* [28]	1.495	1.556	0.041		257.1

Continued on next page

TABLE II – *Continued from previous page*

T^*	Simulation/Theory Group	ρ_l^*	ρ_s^*	$\Delta\rho^*$	L	$P\sigma^3/\epsilon$
-------	-------------------------	------------	------------	----------------	-----	----------------------

NOTE-* indicates values obtained from interpolation of the tabulated values.

TABLE III: Comparison of freezing parameters ρ_l^* , ρ_s^* , $\Delta\rho^*$, Lindemann parameter L and pressure $P^* = P\sigma^3/\epsilon$ found from the present theory with simulations[24–27] and with the RY-DFT and the MWDA[6] for the LJ potential at different values of T^* .

T^*	Simulation/Theory Group	ρ_l^*	ρ_s^*	$\Delta\rho^*$	L	$P\sigma^3/\epsilon$
0.80	Present result (ODS)	0.918	0.976	0.063	0.091	2.57
	Present result (WCAS)	0.892	0.960	0.076	0.091	1.65
	RY-DFT (ODS)	1.009	1.073	0.064	0.074	6.39
	RY-DFT (WCAS)	0.963	1.033	0.073	0.078	3.85
	MC Simulation* [24]	0.878	0.979	0.115		1.39
	MC Simulation [25]	0.891	0.983	0.103		1.65
	MC Simulation* [26]	0.875	0.977	0.117		1.30
	MC Simulation* [27]	0.883	0.979	0.109		1.23
1.00	Present result (ODS)	0.957	1.011	0.056	0.093	5.56
	Present result (WCAS)	0.929	0.994	0.069	0.092	4.18
	RY-DFT (ODS)	1.053	1.115	0.059	0.075	11.14
	RY-DFT (WCAS)	1.001	1.073	0.072	0.077	7.33
	MWDA+MF Theory [6]	0.880	1.025	0.160	0.100	3.20
	MC Simulation* [24]	0.924	1.010	0.094		4.11
	MC Simulation [25]	0.923	1.008	0.092		4.05
	MC Simulation [26]	0.920	1.007	0.095		3.94
MC Simulation* [27]	0.914	1.004	0.099		3.59	
1.35	Present result (ODS)	1.010	1.062	0.052	0.094	11.20
	Present result (WCAS)	0.982	1.045	0.064	0.094	9.11
	RY-DFT (ODS)	1.113	1.178	0.058	0.074	20.03
	RY-DFT (WCAS)	1.063	1.134	0.067	0.077	14.57
	MC Simulation* [24]	0.983	1.061	0.079		9.53
	MC Simulation* [25]	0.973	1.049	0.078		8.99
	MC Simulation* [26]	0.981	1.057	0.077		9.25
	MC Simulation [27]	0.964	1.053	0.092		9.00
1.50	Present result (ODS)	1.028	1.082	0.052	0.095	13.70
	Present result (WCAS)	1.001	1.064	0.063	0.094	11.35
	RY-DFT (ODS)	1.137	1.202	0.057	0.075	24.25
	RY-DFT (WCAS)	1.085	1.157	0.066	0.077	17.92
	MC Simulation* [24]	1.007	1.081	0.074		12.09

Continued on next page

TABLE III – *Continued from previous page*

T^*	Simulation/Theory Group	ρ_l^*	ρ_s^*	$\Delta\rho^*$	L	$P\sigma^3/\epsilon$
	MC Simulation [25]	0.993	1.069	0.077		11.20
	MC Simulation [26]	1.002	1.076	0.074		11.75
	MC Simulation* [27]	0.984	1.073	0.091		11.52
2.00	Present result (ODS)	1.084	1.139	0.052	0.096	22.84
	Present result (WCAS)	1.060	1.120	0.057	0.096	19.76
	RY-DFT (ODS)	1.207	1.271	0.053	0.075	39.60
	RY-DFT (WCAS)	1.155	1.225	0.061	0.077	30.54
	MWDA+MF Theory [6]	1.040	1.140	0.100	0.111	17.70
	MC Simulation* [24]	1.071	1.139	0.064		21.35
	MC Simulation* [25]	1.050	1.124	0.071		19.45
	MC Simulation [26]	1.065	1.134	0.065		20.81
	MC Simulation* [27]	1.042	1.125	0.079		19.59
2.74	Present result (ODS)	1.152	1.207	0.047	0.098	37.86
	Present result (WCAS)	1.126	1.188	0.055	0.098	33.25
	RY-DFT (ODS)	1.288	1.356	0.053	0.075	64.31
	RY-DFT (WCAS)	1.235	1.307	0.058	0.077	51.18
	MC Simulation [24]	1.144	1.211	0.059		36.91
	MC Simulation [25]	1.116	1.181	0.058		33.20
	MC Simulation* [26]	1.139	1.206	0.059		35.95
	MC Simulation [27]	1.113	1.179	0.059		32.20
4.00	Present result (ODS)	1.241	1.297	0.045	0.101	65.82
	Present result (WCAS)	1.216	1.278	0.051	0.100	59.19
	RY-DFT (ODS)	1.400	1.471	0.051	0.074	113.1
	RY-DFT (WCAS)	1.346	1.424	0.058	0.076	92.84
	MC Simulation* [24]	1.245	1.309	0.052		66.78
	MC Simulation [26]	1.237	1.303	0.053		65.37
	MC Simulation* [27]	1.213	1.274	0.050		59.93
5.00	Present result (ODS)	1.297	1.354	0.044	0.102	89.53
	Present result (WCAS)	1.275	1.336	0.048	0.102	82.04
	RY-DFT (ODS)	1.471	1.546	0.051	0.074	155.5
	RY-DFT (WCAS)	1.420	1.495	0.053	0.077	130.6
	MWDA+MF Theory [6]	1.270	1.350	0.060	0.110	79.80
	MC Simulation* [24]	1.306	1.373	0.051		93.13
	MC Simulation [26]	1.300	1.366	0.051		91.20
	MC Simulation [27]	1.279	1.349	0.055		86.00
10.0	Present result (ODS)	1.506	1.562	0.037	0.107	231.3
	Present result (WCAS)	1.485	1.547	0.042	0.107	215.9
	RY-DFT (ODS)	1.729	1.812	0.048	0.074	409.6
	RY-DFT (WCAS)	1.668	1.756	0.053	0.077	347.3
	MWDA+MF Theory [6]	1.530	1.580	0.040	0.104	242.0

Continued on next page

TABLE IV. Comparison of values of $\frac{W_{id}}{N}$, $\frac{W_0}{N}$, and $\frac{W_b}{N}$ at the freezing point for the RLJ potential and for the LJ potential(found from WCAS).

T^*	RLJ Potential				LJ Potential			
	ρ_s^*	$\frac{W_{id}}{N}$	$\frac{W_0}{N}$	$\frac{W_b}{N}$	ρ_s^*	$\frac{W_{id}}{N}$	$\frac{W_0}{N}$	$\frac{W_b}{N}$
0.80	0.988	4.471	-3.972	-0.499	0.960	4.562	-4.115	-0.449
1.00	1.016	4.437	-3.932	-0.506	0.994	4.494	-4.042	-0.454
1.35	1.059	4.372	-3.860	-0.513	1.045	4.419	-3.964	-0.458
1.50	1.075	4.351	-3.839	-0.515	1.064	4.396	-3.938	-0.460
2.00	1.125	4.303	-3.785	-0.520	1.120	4.316	-3.850	-0.468
2.74	1.187	4.235	-3.711	-0.525	1.188	4.246	-3.768	-0.480
4.00	1.274	4.149	-3.620	-0.530	1.278	4.153	-3.660	-0.494
5.00	1.331	4.095	-3.563	-0.533	1.336	4.094	-3.593	-0.502
10.00	1.539	3.919	-3.383	-0.539	1.547	3.918	-3.399	-0.520

TABLE III – *Continued from previous page*

T^*	Simulation/Theory Group	ρ_l^*	ρ_s^*	$\Delta\rho^*$	L	$P\sigma^3/\epsilon$
	MWDA Theory [6]	1.520	1.570	0.030	0.114	237.0
	MC Simulation* [24]	1.530	1.599	0.045		248.0
	MC Simulation [27]	1.500	1.572	0.048		231.0

NOTE-* indicates values obtained from interpolation of the tabulated values.

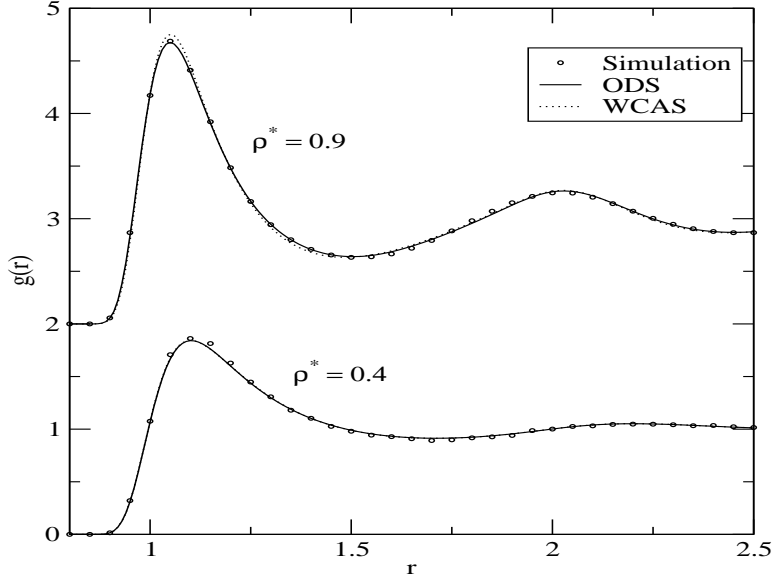


FIG. 1. Comparison of $g^{(0)}(r)$ (r is measured in unit of σ) found from WCAS and ODS of division of LJ potential with the simulation results[22] for $\rho^* = 0.4$ and 0.9 at $T^* = 1.50$.

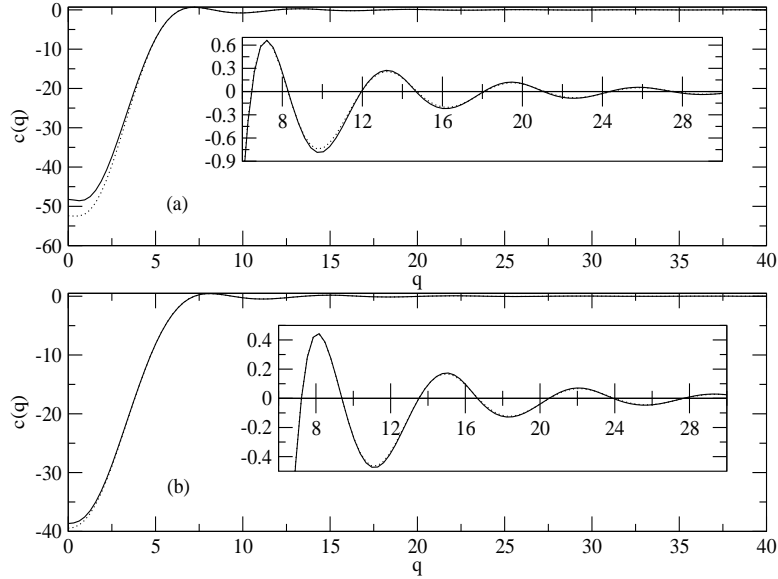


FIG. 2. Comparison between $\hat{c}^{(0)}(q)$ found from WCAS and ODS of division of LJ potential for (a) $\rho^* = 1.05, T^* = 1.50$ and (b) $\rho^* = 1.50, T^* = 10.0$. Full and dotted lines correspond to WCAS and ODS respectively.

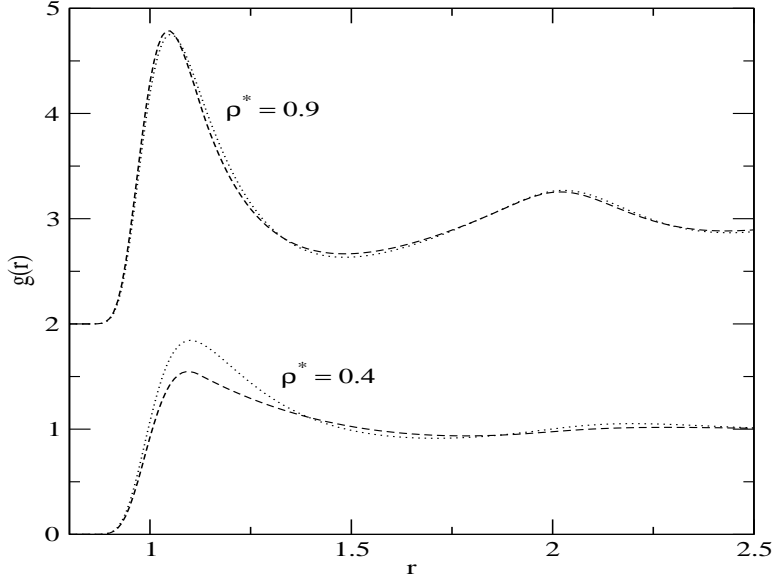


FIG. 3. Comparison of $g^{(0)}(r)$ found from LJ potential(WCAS) and RLJ potential for $\rho^* = 0.4$ and 0.9 at $T^* = 1.50$. The dashed and dotted lines are for the RLJ and LJ potentials respectively

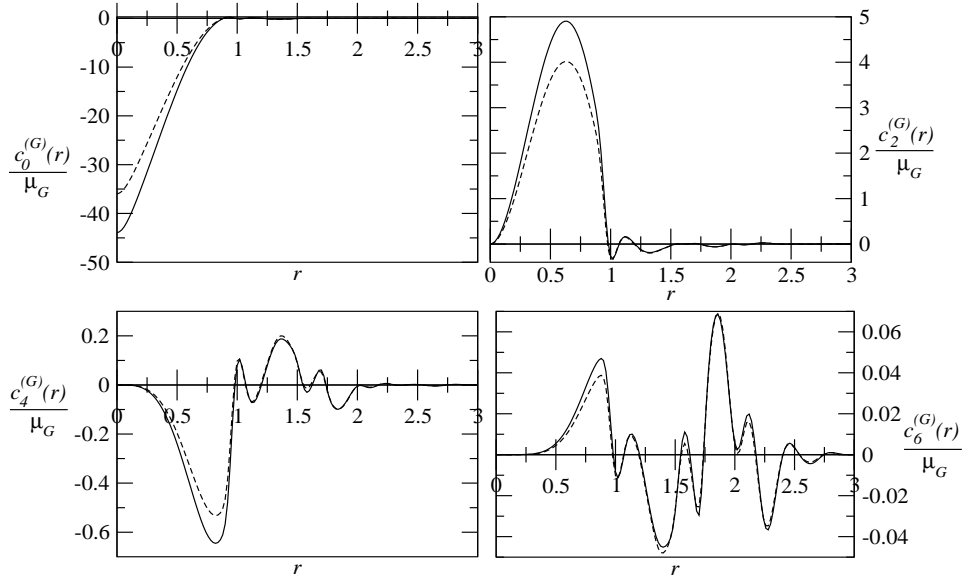


FIG. 4. Comparison of values of $\frac{c_l^{(G)}(r)}{\mu_G}$ as a function of r (measured in unit of σ) for $l = 0, 2, 4$ and 6 for RLJ's of first set of a fcc lattice at $\rho_s^* = 1.10$ and $T^* = 1.50$; the full and dashed lines correspond to LJ (found using WCAS) and RLJ potentials, respectively.

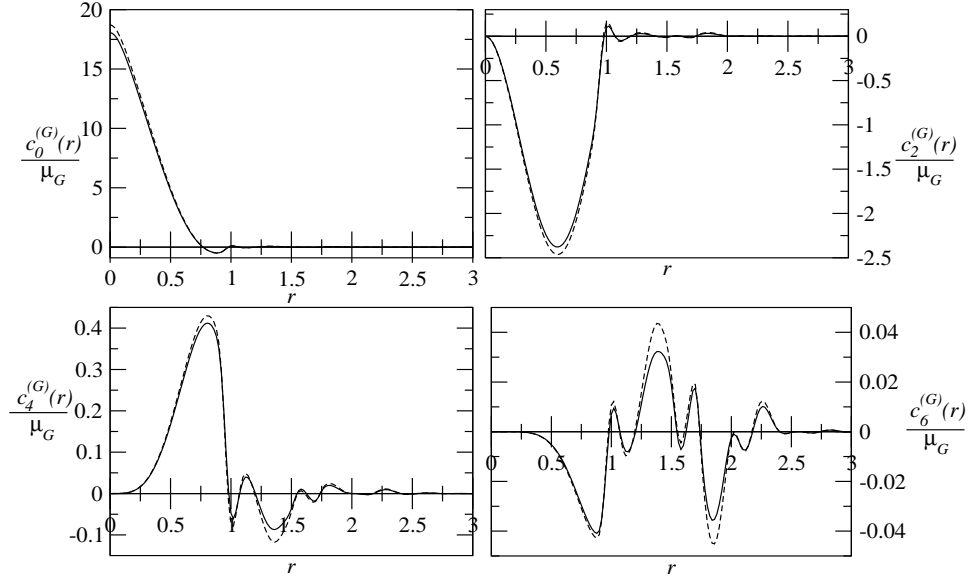


FIG. 5. Same as for Fig.4 but for RLV's of second set of a fcc lattice.

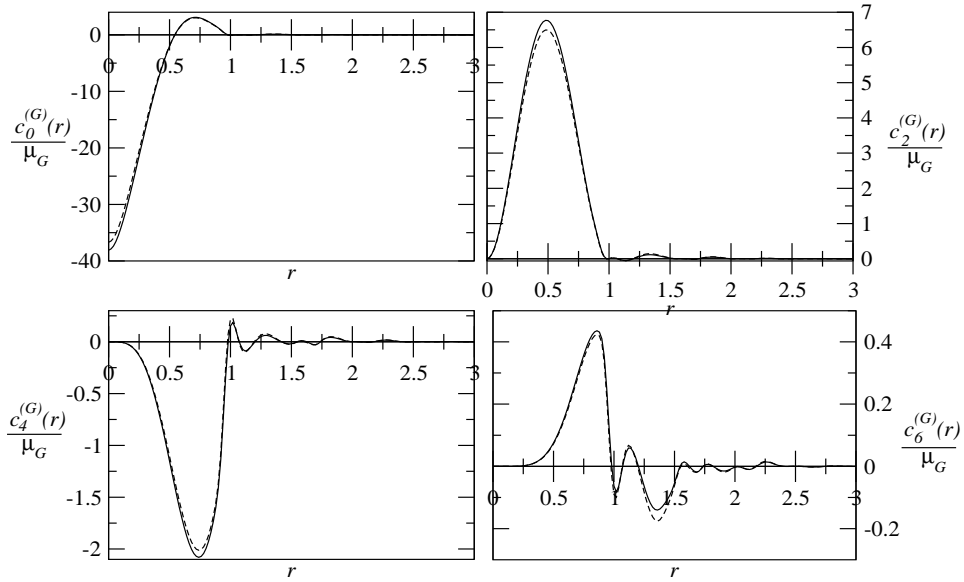


FIG. 6. Same as for Fig.4 but for RLV's of third set of a fcc lattice.

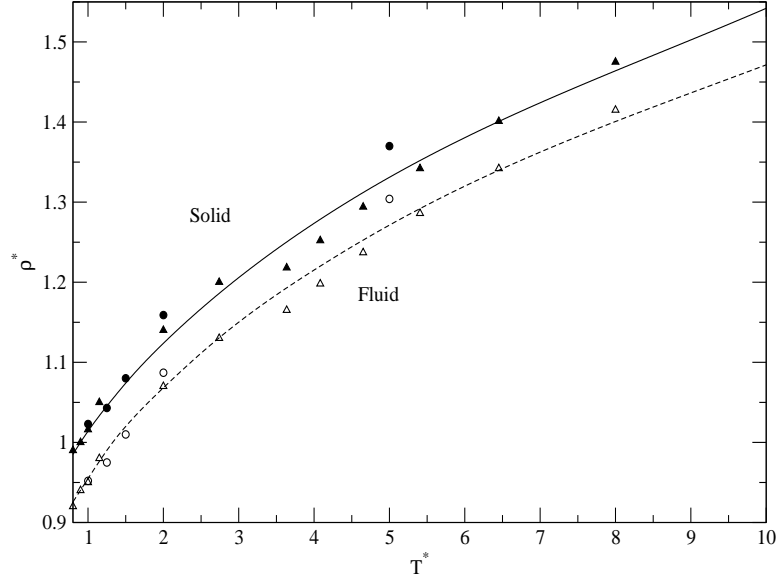


FIG. 7. The $T^* - \rho^*$ phase diagram for the RLJ potential. Full and dashed lines correspond respectively to crystal and fluid at the freezing point, triangles and circles (full for crystal and open for fluid) represent simulation data of refs. [28] and [29] respectively.

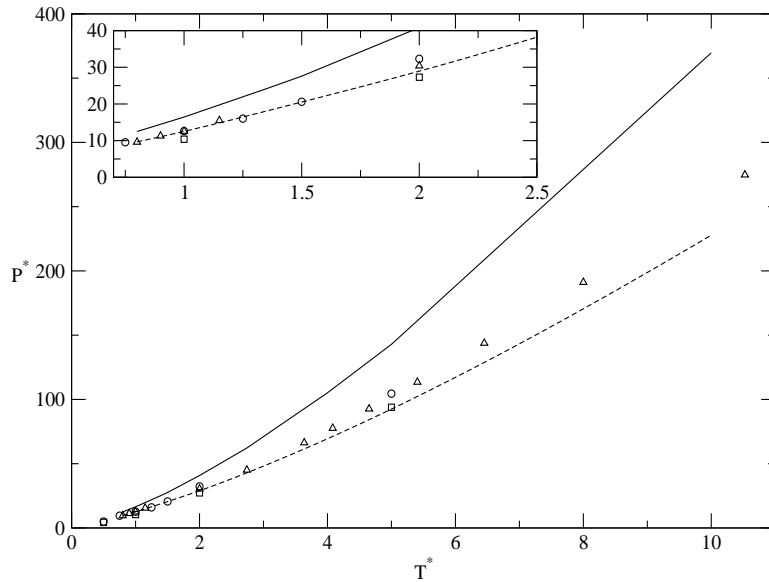


FIG. 8. Pressure P^* vs temperature T^* for RLJ potential. Dashed line represents present data and full line represents data found from RY-DFT, squares represent values from MWDA ([6]) triangles and circles represent simulation data of refs. [28] and [29] respectively.

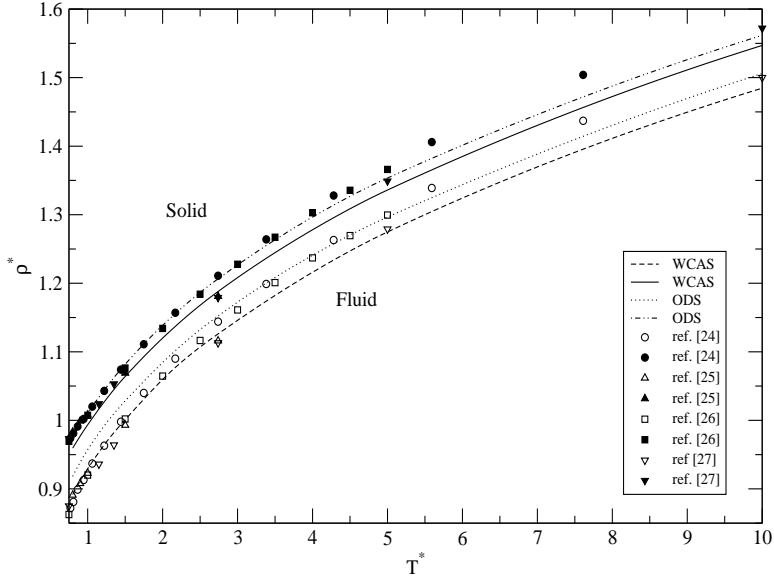


FIG. 9. The $T^* - \rho^*$ phase diagram for the LJ potential in which lines represent present data (calculated via WCAS and ODS) and symbols represent simulation data (full for crystal and open for fluid) found from Agrawal and Kofke [24], Ahmed and Sadus [25], Sousa *et al.* [26] and Hansen [27].

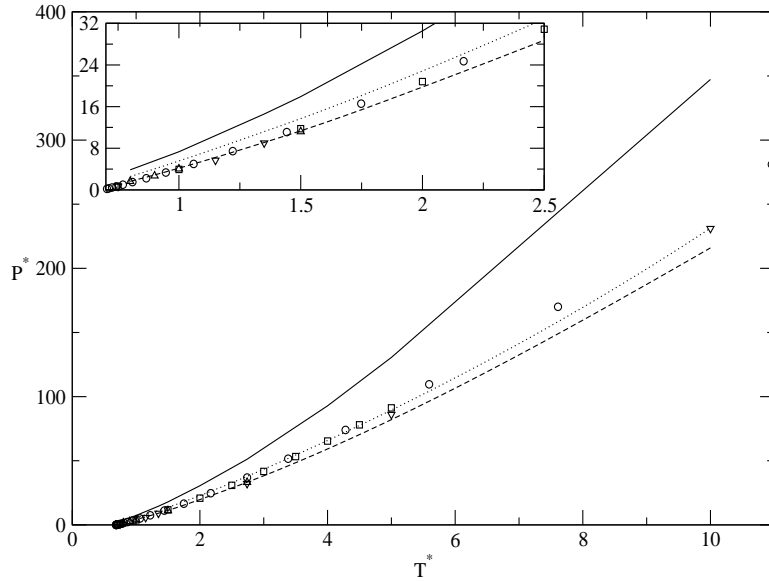


FIG. 10. Pressure P^* vs temperature T^* for LJ potential. Dashed and dotted lines represent present data found from WCAS and ODS division of LJ potential respectively and full line represents data found from RY-DFT. Symbols represent simulation data found from [24–27]; notations are same as in Fig. 9.

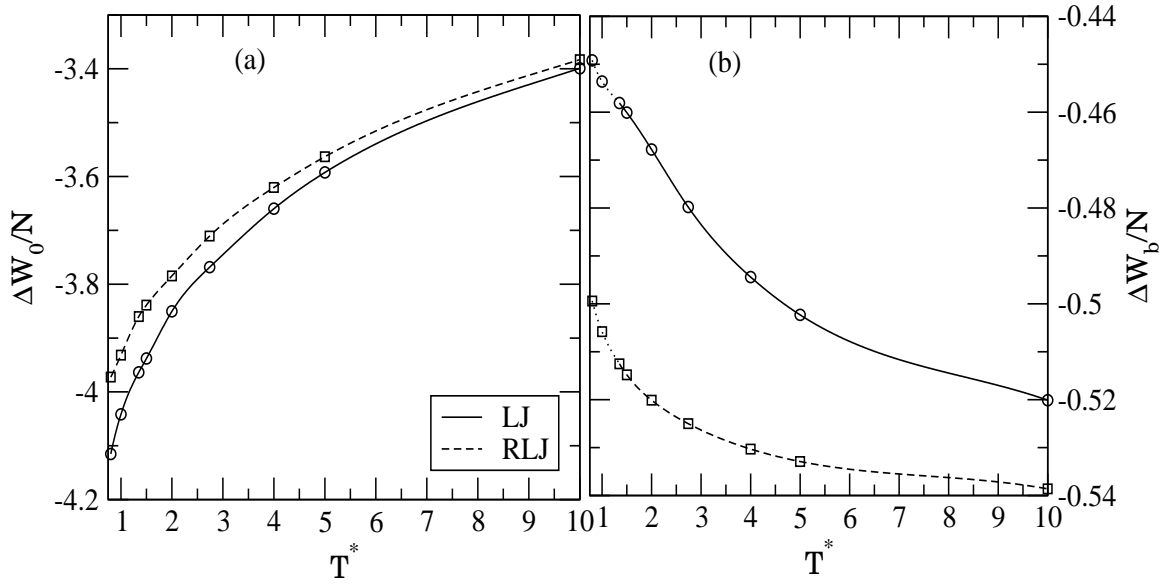


FIG. 11. Comparison of values of $\frac{\Delta W_0}{N}$ and $\frac{\Delta W_b}{N}$ at the freezing points for the LJ (circles) and RLJ (squares) potentials. The dotted part of lines in (b) represent extrapolated values of $\frac{\Delta W_b}{N}$.